

# InAs-Based Single-Mode Distributed Feedback Interband Cascade Lasers

Yuchao Jiang, *Graduate Student Member, IEEE*, Lu Li, Hao Ye, Rui Q. Yang, *Fellow, IEEE*, Tetsuya D. Mishima, Michael B. Santos, Matthew B. Johnson, David Jui-Yang Feng, and Fow-Sen Choa, *Senior Member, IEEE*

**Abstract**—InAs-based single-mode distributed feedback (DFB) interband cascade (IC) lasers were investigated. The DFB grating was patterned using interference lithography to etch the cladding-free upper separate confinement layer of the IC laser structure. Single-mode emission with a side mode suppression ratio of  $\sim 30$  dB was obtained in continuous wave operation at temperatures up to 180 K near 4.5  $\mu\text{m}$ . A total tuning range of 16 nm could be achieved for a single device, with typical temperature- and current-tuning rates of 0.4 nm/K and 0.016 nm/mA, respectively. The impact of the DFB grating on device performance was evaluated and discussed in comparison with Fabry–Perot lasers.

**Index Terms**—Diode lasers, mid-infrared, distributed feedback devices, interband cascade.

## I. INTRODUCTION

INTERBAND cascade (IC) lasers [1], [2] have emerged as efficient mid-infrared (IR) laser sources with low power consumption in the wavelength range from 3 to 6  $\mu\text{m}$  [3]–[8]. To extend beyond 6  $\mu\text{m}$ , IC lasers have been developed on InAs substrates [9]–[14] instead of GaSb substrates that have been used for shorter wavelengths [3]–[8]. By replacing the InAs/AlSb superlattice (SL) cladding layers with highly-doped  $n^+$ -InAs layers, InAs-based IC lasers can have improved optical confinement and thermal dissipation, which has enabled continuous wave (cw) operation at wavelengths as long as 11  $\mu\text{m}$  [14]. InAs-based IC lasers can also cover the mid-IR region for the detection of important molecules such as CO<sub>2</sub> (4.3  $\mu\text{m}$ ), carbonyl sulfide/COS (4.5  $\mu\text{m}$ ), CO (4.6  $\mu\text{m}$ ), N<sub>2</sub>O (4.8  $\mu\text{m}$ ), and NO (5.2  $\mu\text{m}$ ). For sensitive detection, single-mode IC lasers are highly desirable for tunable laser

Manuscript received June 13, 2015; revised August 6, 2015; accepted August 12, 2015. Date of publication September 1, 2015; date of current version September 3, 2015. This work was supported by the National Science Foundation through the Division of Electrical, Communications and Cyber Systems under Grant ECCS-1002202.

Y. Jiang, L. Li, H. Ye, and R. Q. Yang are with the School of Electrical and Computer Engineering, University of Oklahoma, Norman, OK 73019 USA (e-mail: jychstar@gmail.com; llu@ou.edu; yehao@ou.edu; rui.q.yang@ou.edu).

T. D. Mishima, M. B. Santos, and M. B. Johnson are with the Homer L. Dodge Department of Physics and Astronomy, University of Oklahoma, Norman, OK 73019 USA (e-mail: mishima@ou.edu; msantos@ou.edu; matthew.b.johnson-2@ou.edu).

D. J.-Y. Feng was with the Department of Computer Science and Electrical Engineering, University of Maryland at Baltimore County, Baltimore, MD 21250 USA. He is now with the Department of Electrical Engineering, National University of Kaohsiung, Taiwan (e-mail: djyfeng@gmail.com).

F.-S. Choa is with the Department of Computer Science and Electrical Engineering, University of Maryland at Baltimore County, Baltimore, MD 21250 USA (e-mail: choa@umbc.edu).

Color versions of one or more of the figures in this paper are available online at <http://ieeexplore.ieee.org>.

Digital Object Identifier 10.1109/JQE.2015.2470534

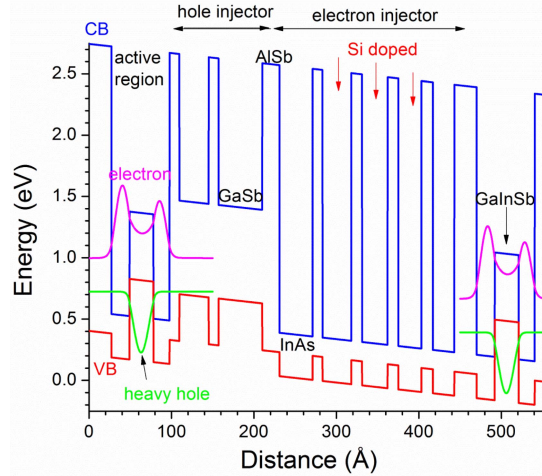


Fig. 1. Band-edge diagram for one cascade stage of the interband cascade laser and calculated wavefunctions in the active regions.

absorption spectroscopy [15]. GaSb-based single-mode distributed feedback (DFB) IC lasers have been developed for detection of important molecules such as CH<sub>4</sub>, C<sub>2</sub>H<sub>6</sub> and H<sub>2</sub>CO [16]–[20]. In this work, we report the first demonstration of InAs-based single-mode DFB IC lasers, which are tunable over 16 nm near 4.5  $\mu\text{m}$ . The device performance of the DFB lasers is evaluated and discussed in comparison with corresponding Fabry–Perot (FP) lasers.

## II. IC LASER STRUCTURE

The laser structure was designed to have 8 cascade stages and grown in a molecular beam epitaxy (MBE) system on an  $n^+$ -type InAs (001) epi-ready substrate, which was labeled as wafer R087. The growth rates of InAs for this IC laser structure were 0.22 and 0.66 ML/s for cascade stages and other regions, respectively [21]. The schematic band-edge diagram of the cascade stage is shown in Figure 1, with calculated electron/hole wavefunctions based on a two-band model [22], [23]. One cascade stage comprises an active region, a hole injector and an electron injector, which are made of AlSb/InAs/GaInSb/InAs/AlSb quantum wells (QWs), two AlSb/GaSb QWs, and five InAs/AlSb QWs, respectively. Some InAs QW layers in the electron injector were doped with Si to  $4.3 \times 10^{18} \text{ cm}^{-3}$  for “carrier rebalancing” [4]. The 8 cascade stages in total were sandwiched between 1.2- $\mu\text{m}$ -thick bottom and 1.5- $\mu\text{m}$ -thick top nominally undoped  $n$ -type InAs separate confinement layers (SCLs). Together they formed the waveguide core, which, in turn, was sandwiched between 1.6- $\mu\text{m}$ -thick highly doped  $n^+$ -type InAs bottom cladding and 35-nm-thick  $n^+$ -InAs top contact layers (doped

with Si to  $1.0 \times 10^{19} \text{ cm}^{-3}$ ). Additionally, a 10-nm-thick n-type InAs layer (doped to  $4.3 \times 10^{18} \text{ cm}^{-3}$ ) was inserted as a transition layer between the SCL and the n<sup>+</sup>-type InAs bottom cladding (and the top contact) layer.

This IC laser structure with thin top contact and transition layers does not have a regular top semiconductor cladding. Nevertheless, when it is incorporated into a hybrid waveguide with a top dielectric layer (SiO<sub>2</sub> or Si<sub>3</sub>N<sub>4</sub> layer), it can achieve better device performance compared to an IC laser with a regular cladding structure as we previously demonstrated [10]. Even without the top dielectric layer, our simulation suggested that the device performance with an appropriate metal cladding layer can still be comparable to an IC laser with the regular top cladding structure [10]. Consequently, this top semiconductor cladding-free IC laser structure should allow a top DFB grating that can be simply integrated into the structure and results in large coupling coefficient.

### III. DEVICE FABRICATION AND EXPERIMENT

Part of the wafer was first processed into broad-area (150-μm-wide) mesa FP devices (without a DFB grating) by contact photolithography and wet-chemical etching. The etching depth reached the bottom SCL to prevent lateral current spreading. A 200-nm-thick, 90-μm-wide SiO<sub>2</sub> insulating layer was deposited on the center of the mesa stripe, followed by the sputter deposition of a 30/300-nm-thick, 100-μm-wide Ti/Au layer for current injection. The laser geometry is the same as that in Figure 3 of Ref [14]. The processed wafer was cleaved into laser bars with cavity lengths of 1 to 2 mm, the facets were left uncoated, and the devices were mounted epi-side-up. The laser bars were placed on the cold finger of a cryostat for measurements in cw and pulsed modes. A representative 2-mm-long device lased at temperatures up to 231 K in cw mode near 4.9 μm (~4.3 μm at 80 K) and 320 K in pulsed mode near 5.0 μm (This result will be compared to our DFB lasers below). At 300 K, this laser had a threshold current density of 600 A/cm<sup>2</sup> with a voltage efficiency of 70%. These characteristics indicate that the material quality is good enough for DFB lasers.

After the FP lasers were evaluated, two pieces of the wafer were separately processed into DFB lasers. The DFB grating period  $\Lambda$  was designed according to the standard first-order grating equation:

$$\lambda = 2\Lambda N_{eff}, \quad (1)$$

where  $N_{eff}$  is the effective index of the laser waveguide and  $\lambda$  is the lasing wavelength. The FP laser mentioned above had a temperature tuning rate of ~3.2 nm/K, which is mainly determined by the temperature dependence of the bandgap of the semiconductor material. In contrast, the wavelength tuning of a DFB laser is dominated by the less temperature sensitive effective index ( $dN_{eff}/dT = 2$  to  $3 \times 10^{-4}$ ). This means, a DFB laser only operates in a relatively narrow temperature window with single mode output. In order to have a reasonable tuning range, we chose an intermediate cw operating temperature of 160 K with a corresponding target wavelength of 4.45 μm. Waveguide simulations calculated an

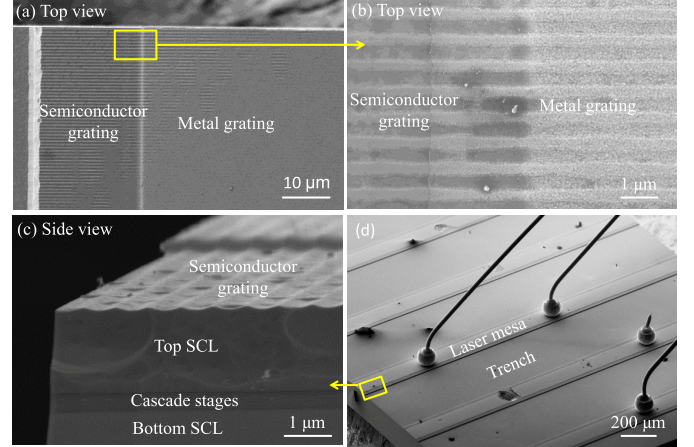


Fig. 2. Scanning electron microscope (SEM) images of IC laser structures. (a) a top view of the DFB gratings covered with metal and without metal; (b) zoom-in of the DFB grating; (c) cross-sectional view of a laser, in which 8 cascade stages are identified below the top SCL; and (d) the top view of a laser mesa, which is mostly metal covered for bonding.

effective index of ~3.4 for our laser structure. Using (1), the designed grating period is 655 nm. To simplify the device fabrication in this initial attempt, gratings were only covered by metal without a dielectric layer. A finite-element simulation gave a coupling coefficient ( $\kappa$ ) of ~12 cm<sup>-1</sup> for a rectangular grating with a depth of 100 nm and a duty cycle of 50%. A 1-mm-long DFB laser can have a decent coupling strength (*i.e.*  $|\kappa L| > 1$ ). Note that in this case both index coupling and loss coupling exist because of the large imaginary part of the refractive index for a metal.

The DFB gratings were defined using interference lithography and Cl<sub>2</sub> reactive ion etching (RIE) to etch the grating into the top InAs SCL. These DFB samples were processed into broad-area lasers by contact photolithography and wet chemical etching. Without a dielectric layer on the top, 30/300 nm-thick Ti/Au layers were directly deposited on the top grating for complex index coupling as well as electrical injection. After substrate lapping and deposition of a back metal contact, the wafers were cleaved into laser bars with cavity lengths of 1 to 2 mm without facet coatings. These DFB lasers were mounted epi-side-up on a Cu-heatsink for measurements. SEM images of typical lasers with magnifications of critical regions are shown in Figure 2. As shown in Figures 2(a) and (d), the top metal stripes were narrower than the mesa width to prevent the metal contact layer from covering to the sidewall. However, the majority of the grating regions are covered by these metal layers to ensure sufficient complex index coupling. As seen in Figure 2(b), the grating stripes are essentially periodic, although there are some variations and non-uniformity. In Figure 2(c), 8 cascade stages can be clearly identified below the top SCL. The surface DFB gratings have a depth of about 100 nm and a duty cycle of about 35%. The grating period is  $595 \pm 5$  nm for the first and  $640 \pm 5$  nm for the second laser samples, respectively.

### IV. EXPERIMENTAL RESULTS AND DISCUSSION

Lasers from the first DFB sample (grating period of ~595 nm) had a grating period that was significantly

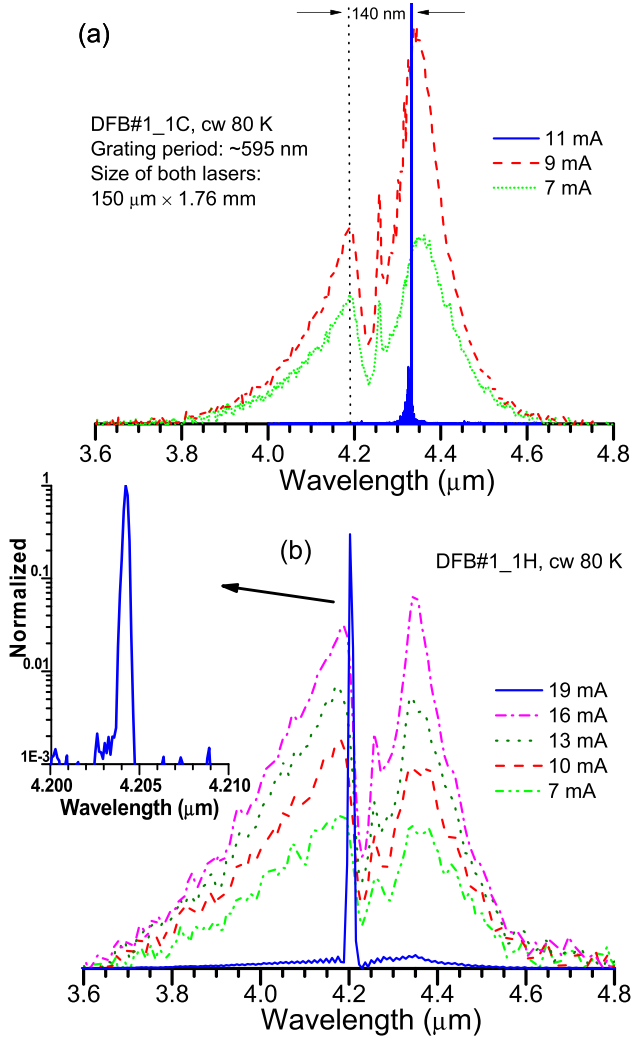


Fig. 3. Emission spectra from two  $150 \mu\text{m} \times 1.76 \text{ mm}$  IC lasers with a grating period of  $\sim 595 \text{ nm}$  at  $80 \text{ K}$  for several currents using (a) device C; and (b) device H, with a log intensity plot inset.

shorter than the designed value (655 nm). As expected, most of these lasers didn't achieve single-mode operation, because the wavelength determined by DFB grating was not aligned with the gain peak (see Figure 3 (a) for device C). Two emission peaks separated by about 140 nm could be identified in the sub-threshold spectra. The two distinctive dips around  $4.3 \mu\text{m}$  are due to the strong absorption of  $\text{CO}_2$ . Nevertheless because of material non-uniformity and/or variations of the DFB grating period, a few lasers did exhibit single-mode operation at  $80 \text{ K}$ . The gain peak for these devices happened to be close to the wavelength of the DFB mode, as shown in Figure 3(b) for device H. The electroluminescent intensity for device H increased with current at a much slower rate than that for device C (without lasing at the DFB wavelength), which resulted in a higher threshold current density ( $7 \text{ A/cm}^2$  vs.  $4 \text{ A/cm}^2$ ). The differences in lasing wavelength and threshold current density between device C and H in a wide temperature range are shown later in Figure 8.

Nevertheless, when device H lased at  $80 \text{ K}$ , the side modes around the DFB mode ( $4.204 \mu\text{m}$ ) were suppressed with a side

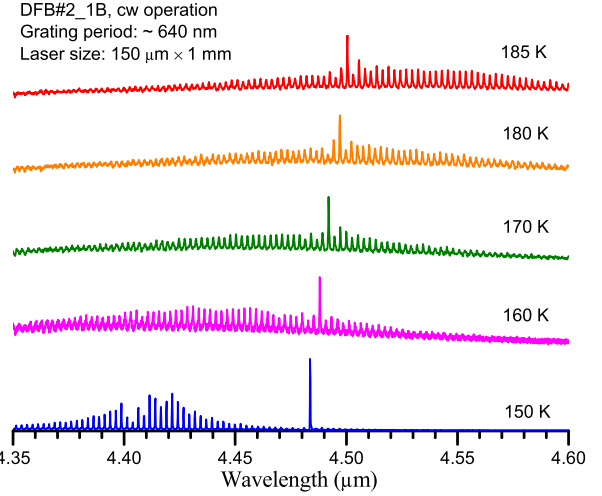


Fig. 4. Sub-threshold emission spectra collected from a broad-area DFB IC laser with a grating period of  $\sim 640 \text{ nm}$  at heat-sink temperatures ranging from  $150$  to  $185 \text{ K}$ .

mode suppression ratio (SMSR) of about  $30 \text{ dB}$  (see inset to Figure 3 (b)). For device H, single DFB-mode behavior was observed at  $90 \text{ K}$  with a SMSR larger than  $20 \text{ dB}$ , which existed simultaneously with FP modes at a relatively high current. Using (1), the effective index is  $3.53 \pm 0.04$  at  $80 \text{ K}$ . The extracted effective index is higher than the value calculated for this laser layer structure. Currently, this is not understood: it may be related to the complex refractive index in metals and/or variations and non-uniformity of the DFB gratings.

The devices from the second DFB processing (grating period  $\sim 640 \text{ nm}$ ) exhibited robust single-mode lasing at higher temperatures. The sub-threshold emission spectra for a 1-mm-long device at several temperatures (see Fig. 4) indicate that the laser gain spectrum is well aligned with the DFB mode at a wavelength of  $4.48 \mu\text{m}$  at temperatures above  $150 \text{ K}$ . Above threshold, mode-hop-free single-frequency lasing emission was observed in a temperature range of  $150$  to  $180 \text{ K}$ . Figure 5 shows typical current-tuning spectra for this device at  $160 \text{ K}$ , with a SMSR of about  $30 \text{ dB}$  (inset Figure 5) and a current-tuning rate of  $16 \text{ nm/A}$  in the vicinity of  $4.49 \mu\text{m}$ . The tuning range is about  $2 \text{ nm}$  when the current was raised from  $140$  to  $260 \text{ mA}$  at  $160 \text{ K}$ . This tuning is mainly attributed to Joule heating from current injection. Hence, the tuning range can be expanded with more current injection.

Figure 6 shows the single-mode emitting wavelengths measured for the same laser operating at various heat-sink temperatures and injection currents. The extracted average temperature-tuning rate of the DFB wavelengths was  $0.4 \text{ nm/K}$ . Together with the current tuning, a total tuning range of  $16 \text{ nm}$  was achieved for a single device, which is sufficient for covering a specific absorption spectral region of a gas molecule. The current-voltage-light characteristics in the corresponding temperature range are shown in Figure 7. The output power emitted from one facet of the device was larger than  $1 \text{ mW}$  at  $180 \text{ K}$  near  $4.50 \mu\text{m}$ , which can satisfy the

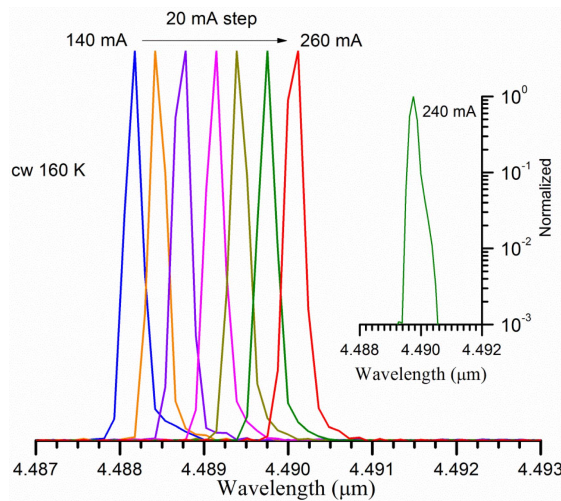


Fig. 5. Current-tuning cw spectra of the DFB IC laser at 160 K, with an SMSR of about 30 dB. Inset is a log intensity plot.

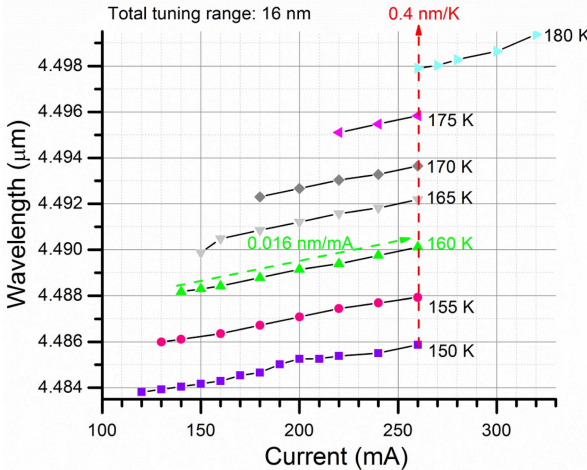


Fig. 6. Single-mode lasing wavelengths of a DFB IC laser as a function of injected currents for temperatures between 150 and 180 K. A total tuning range of 16 nm was achieved for a single device, with temperature- and current-tuning rates of 0.4 nm/K and 0.016 nm/mA, respectively. Only data for which the spectral SMSR was at least 20 dB are included.

requirement for in situ sensing. Note that the collected power was only calibrated for the 10% transmission loss from the  $\text{CaF}_2$  window of the cryostat, without considering the beam divergence. Hence, the actual output power should be higher than the reported values in Figure 7. The inset to Figure 7 shows the lasing spectra of the DFB mode at temperatures from 150 to 180 K. The extracted effective index is  $3.54 \pm 0.04$  (with a temperature coefficient of  $dN_{eff}/dT = 3.6 \times 10^{-4}$ ), which is again higher than our previous estimate based on the laser layer structure. These experimental values will help improve the accuracy in our future design.

Above 185 K, the DFB mode became detuned away from the gain spectral peak and the laser operation was based on FP modes. If the DFB grating is designed to aim at a longer wavelength (corresponding to the higher temperature) and narrow-ridge lasers are fabricated from this same wafer,

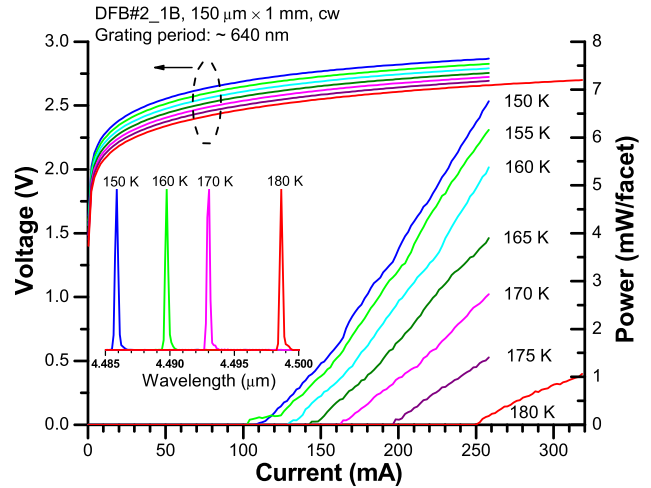


Fig. 7. Current-voltage-light characteristics for a DFB IC laser. Inset: cw spectra at temperatures from 150 to 180 K.

cw operation based on the DFB mode near  $5 \mu\text{m}$  would be achievable at  $\sim 270$  K. The expected device performance from this InAs-based wafer is still no better than the state-of-the-art GaSb-based DFB IC lasers [18]–[20]. However, these results are helpful to assess how InAs-based DFB lasers can be further developed considering that a recent innovative design of the waveguide has brought InAs-based IC lasers to a new performance level [24].

To evaluate how DFB gratings can affect the device performance, InAs-based IC lasers with and without DFB gratings are compared in terms of their temperature dependent lasing wavelengths and threshold current densities in cw mode, as shown in Figure 8. Because the longer cavity length will lead to less mirror loss and thus lower threshold current density, the FP lasers with two different lengths are plotted as reference lasers (open symbols). As shown in Figure 8, the devices that lased with DFB modes (solid symbols) had higher threshold current densities than the FP lasers. The laser with the widest DFB tuning range had the highest threshold current density. This suggests that the optical coupling with the grating contributed significant extra loss, or the differential gain at the DFB wavelength is smaller, or a combination of both factors. Also shown in Figure 8, a laser with the grating but no lasing at the DFB mode (half-filled symbol), had a similar threshold current density as the FP laser of a similar length. This implies that the metal grating itself might not have a substantial effect on the FP laser performance, which is worth further exploration. A way to further eliminate the possible loss is to insert a dielectric layer between the grating and the metal, which will be investigated in our future effort.

It should be noted that the DFB mode from a broad-area laser device is a single mode in the longitudinal direction, but may contain multiple lateral modes along the mesa perpendicular to the longitudinal direction [25]–[27]. This is because a wide ( $150\text{-}\mu\text{m}$  in this work) mesa allows multiple lateral modes to coexist with more densely distributed longitudinal cavity modes. Consequently, the emission spectrum from a broad-area laser looks like a superposition of multiple

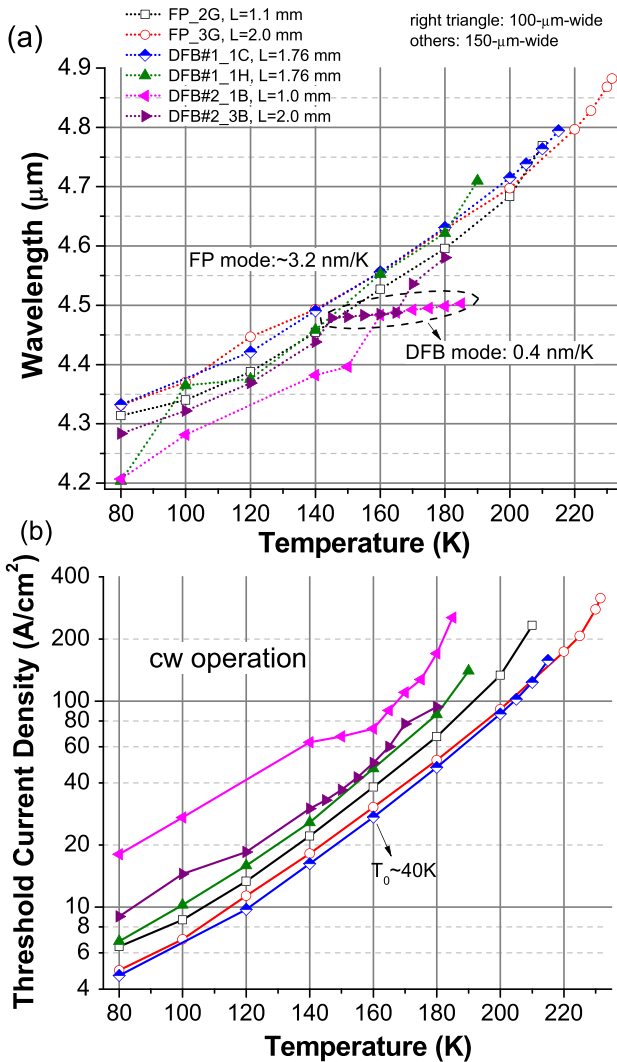


Fig. 8. Comparisons of FP and several DFB lasers at various cw operating temperatures in terms of: (a) lasing wavelengths; (b) threshold current densities.

frequency combs. Hence, at the location of the DFB grating determined frequency (wavelength), there could be an overlap of several modes from different lateral branches. The observed lateral far-field profile of a DFB laser (the device in Fig. 4) had a full width at the half maximum (FWHM) of about  $13^\circ$ . This value is much larger than the estimated value of  $\sim 4^\circ$  based only on the fundamental lateral mode, suggesting a superposition of several lateral modes [28] at the DFB wavelength. A single fundamental lateral mode can be obtained either by narrowing the ridge [3] or by introducing additional loss to the higher-order modes [19].

## V. SUMMARY

In summary, InAs-based single-mode DFB IC lasers have been demonstrated in cw operation with a high SMSR ( $\sim 30$  dB) at temperatures up to 180 K near  $4.5\ \mu\text{m}$ . With the metal contact layer directly deposited on the top DFB grating for complex coupling, a large tuning range of 16 nm was achieved. Also, the DFB laser performance was compared with

the corresponding FP laser performance to identify aspects that need to be improved. It is expected that high performance InAs-based single-mode DFB lasers will be realized for practical applications with further efforts to advance understanding of the device operation, device fabrication and material quality.

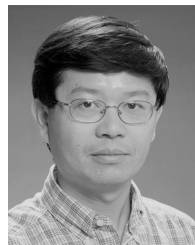
## ACKNOWLEDGMENT

The authors are grateful to S. Rassel and L. Zhao for their technical assistance.

## REFERENCES

- [1] R. Q. Yang, "Infrared laser based on intersubband transitions in quantum wells," *Superlattices Microstruct.*, vol. 17, no. 1, pp. 77–83, Jan. 1995.
- [2] R. Q. Yang, "Interband cascade (IC) lasers," in *Semiconductor Lasers: Fundamentals and Applications*, A. Baranov and E. Tournie, Eds. Cambridge, U.K.: Woodhead Publishing, 2013.
- [3] W. Bewley *et al.*, "Ridge-width dependence of midinfrared interband cascade laser characteristics," *Opt. Eng.*, vol. 49, no. 11, p. 111116, Nov. 2010.
- [4] I. Vurgaftman *et al.*, "Rebalancing of internally generated carriers for mid-infrared interband cascade lasers with very low power consumption," *Nature Commun.*, vol. 2, p. 585, Dec. 2011.
- [5] I. Vurgaftman *et al.*, "Interband cascade lasers with low threshold powers and high output powers," *IEEE J. Sel. Topics Quantum Electron.*, vol. 19, no. 4, Jul./Aug. 2013, Art. ID 1200210.
- [6] R. Weih, M. Kamp, and S. Höfling, "Interband cascade lasers with room temperature threshold current densities below  $100\ \text{A}/\text{cm}^2$ ," *Appl. Phys. Lett.*, vol. 102, no. 23, p. 231123, 2013.
- [7] C. L. Canedy *et al.*, "Pulsed and CW performance of 7-stage interband cascade lasers," *Opt. Exp.*, vol. 22, no. 7, pp. 7702–7710, 2014.
- [8] I. Vurgaftman *et al.*, "Interband cascade lasers," *J. Phys. D, Appl. Phys.*, vol. 48, no. 12, p. 123001, 2015.
- [9] Z. Tian *et al.*, "InAs-based interband cascade lasers near  $6\ \mu\text{m}$ ," *Electron. Lett.*, vol. 45, no. 1, pp. 48–49, 2009.
- [10] Z. Tian *et al.*, "InAs-based mid-infrared interband cascade lasers near  $5.3\ \mu\text{m}$ ," *IEEE J. Quantum Electron.*, vol. 48, no. 7, pp. 915–921, Jul. 2012.
- [11] R. Q. Yang *et al.*, "Recent progress in development of InAs-based interband cascade lasers," in *Proc. SPIE*, vol. 8640, paper 86400Q, Mar. 2013.
- [12] M. Dallner, S. Höfling, and M. Kamp, "Room-temperature operation of InAs-based interband-cascade-lasers beyond  $6\ \mu\text{m}$ ," *Electron. Lett.*, vol. 49, no. 4, pp. 286–287, Feb. 2013.
- [13] M. Dallner, F. Hau, S. Höfling, and M. Kamp, "InAs-based interband-cascade-lasers emitting around  $7\ \mu\text{m}$  with threshold current densities below  $1\ \text{kA}/\text{cm}^2$  at room temperature," *Appl. Phys. Lett.*, vol. 106, no. 4, p. 041108, 2015.
- [14] L. Li *et al.*, "MBE-grown long-wavelength interband cascade lasers on InAs substrates," *J. Crystal Growth*, vol. 426, pp. 369–372, Sep. 2015.
- [15] C. R. Webster *et al.*, "Mars methane detection and variability at Gale crater," *Science*, vol. 347, no. 6220, pp. 415–417, 2015.
- [16] R. Q. Yang *et al.*, "Distributed feedback mid-IR interband cascade lasers at thermoelectric cooler temperatures," *IEEE J. Sel. Topics Quantum Electron.*, vol. 13, no. 5, pp. 1074–1078, Sep./Oct. 2007.
- [17] G. Wysocki *et al.*, "Dual interband cascade laser based trace-gas sensor for environmental monitoring," *Appl. Opt.*, vol. 46, no. 33, pp. 8202–8210, 2007.
- [18] M. von Edlinger *et al.*, "Monomode interband cascade lasers at  $5.2\ \mu\text{m}$  for nitric oxide sensing," *IEEE Photon. Technol. Lett.*, vol. 26, no. 5, pp. 480–482, Mar. 1, 2014.
- [19] C. S. Kim *et al.*, "Corrugated-sidewall interband cascade lasers with single-mode midwave-infrared emission at room temperature," *Appl. Phys. Lett.*, vol. 95, no. 23, p. 231103, 2009.
- [20] J. Koeth *et al.*, "Distributed feedback interband cascade lasers for applications in research and industry," in *Proc. SPIE*, vol. 9382, paper 93820V, Mar. 2015.
- [21] H. Ye *et al.*, "MBE growth optimization of InAs (001) homoepitaxy," *J. Vac. Sci. Technol. B*, vol. 31, no. 3, p. 03C135, 2013.
- [22] R. Q. Yang and J. M. Xu, "Analysis of transmission in polytype interband tunneling heterostructures," *J. Appl. Phys.*, vol. 72, no. 10, p. 4714, 1992.
- [23] R. Q. Yang and J. M. Xu, "Bound and quasibound states in leaky quantum wells," *Phys. Rev. B*, vol. 46, p. 6969, Sep. 1992.

- [24] L. Li *et al.*, "Low-threshold InAs-based interband cascade lasers operating at high temperatures," *Appl. Phys. Lett.*, vol. 106, no. 25, p. 251102, 2015.
  - [25] C. J. Chang-Hasnain, E. Kapon, and R. Bhat, "Spatial mode structure of broad-area semiconductor quantum well lasers," *Appl. Phys. Lett.*, vol. 54, no. 3, p. 205, 1989.
  - [26] M. Kanskar *et al.*, "53% wallplug efficiency 975nm distributed feedback broad area laser," *Electron. Lett.*, vol. 42, no. 25, pp. 1455–1457, Dec. 2006.
  - [27] C. M. Schultz, P. Crump, H. Wenzel, O. Brox, F. Bugge, and G. Erbert, "Narrow vertical far-field 975-nm broad-area DFB lasers for wide temperature range operation," *IEEE Photon. Technol. Lett.*, vol. 21, no. 9, pp. 593–595, May 1, 2009.
  - [28] Z. Yin *et al.*, "Far-field patterns of plasmon waveguide interband cascade lasers," *IEEE J. Quantum Electron.*, vol. 47, no. 11, pp. 1414–1419, Nov. 2011.



**Rui Q. Yang** (M'95-SM'02-F'14) received the B.Sc. degree in physics from Zhejiang University, Hangzhou, China, in 1982, and the Ph.D. degree in physics from Nanjing University, Nanjing, China, in 1987.

A black and white portrait of Dr. Ming Tang, a middle-aged man with short dark hair, wearing glasses and a plaid button-down shirt. He is looking directly at the camera with a neutral expression.

He was a Principal Member of the Engineering Staff and a Task Manager with the Jet Propulsion Laboratory (JPL), Pasadena, CA. He joined the University of Oklahoma (OU), in 2007. He is currently a Professor with the School of Electrical and Computer Engineering, OU, with research activities

ranging from condensed matter physics to semiconductor quantum devices, such as mid-infrared lasers, detectors, and photovoltaic devices.

such as mid-infrared lasers, detectors, and photovoltaic devices.

Prof. Yang has authored/co-authored more than 120 refereed journal articles and two book chapters. He is a fellow of the Optical Society. He received the Edward Stone Award from JPL for outstanding research publication and the successful accelerated infusion of cutting-edge interband cascade semiconductor laser technology into flight mission readiness in 2007.



cascade lasers.

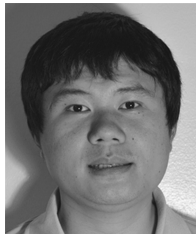
**Yuchao Jiang** (GSM'15) received the B.S. degree in applied physics from the Beijing University of Posts and Telecommunications, in 2007, and the M.S. degree in material physics and chemistry from the Institute of Semiconductors, Chinese Academy of Sciences, Beijing, China, in 2011.

He is currently pursuing the Ph.D. degree in electrical and computer engineering with the University of Oklahoma, Norman. His research interests include modeling and characterization of infrared optoelectronic devices, including quantum and interband



**Tetsuya D. Mishima** received the Ph.D. degree from Waseda University, Tokyo, Japan, in 1999. He has been a Research Scientist with the University of Oklahoma, Norman, since 2001.

He held a post-doctoral position with Pennsylvania State University, University Park, from 1999 to 2001. He has co-authored about 70 scientific publications. His current research interests include structural defect reduction in semiconductor structures grown by molecular beam epitaxy, development of transmission electron microscopy techniques for struc-



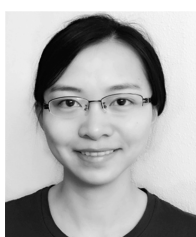
Post-Doctoral Researcher with the University of Oklahoma, Norman. He has authored/co-authored over 80 scientific publications. His current research interests include infrared optoelectronic materials and devices, including lasers, photodetectors, and photovoltaics based on interband cascade structure.

in 2008. He was an Assistant Research Fellow with the Institute of Semiconductors, Chinese Academy of Sciences, from 2008 to 2012. He is currently with Dr. Yang's and Dr. Santos's groups as a Post-Doctoral Researcher with the University of



**Michael B. Santos** received the B.S. degree in electrical engineering and materials science from Cornell University, Ithaca, NY, in 1986, and the Ph.D. degree in electrical engineering from Princeton University, Princeton, NJ, in 1992.

He was a Post-Doctoral Researcher with AT&T Bell Laboratories, Holmdel, NJ, before joining the University of Oklahoma, Norman, in 1993. He is currently a Professor of Physics with the University of Oklahoma. He has co-authored 230 papers in experimental semiconductor research.



**Hao Ye** received the B.S. degree in electronics engineering from East China Normal University, Shanghai, China, in 2010, and the M.S. degree in electrical and computer engineering from the University of Oklahoma, Norman, in 2012.

She is currently pursuing the Ph.D. degree with the University of Oklahoma. Her current research interests include molecular beam epitaxy growth and characterization of III-V devices, in particular, the interband cascade lasers, detectors, and thermophotovoltaics.



**Matthew B. Johnson** received the B.S. degree in physics from the University of Waterloo, Waterloo, ON, Canada, in 1979, and the Ph.D. degree in applied physics from the California Institute of Technology, Pasadena, in 1989.

He held post-doctoral positions with IBM Research, Yorktown Heights, NY, and IBM Research, Zürich, Switzerland. He has been a Physics Faculty Member with the University of Oklahoma, Norman, since 1995. He has served as the Director of the Center for Semiconductor Materials, the National Science Foundation Materials Engineering Center, University of Oklahoma, with University of Arkansas, Fayetteville, since 2000. He has scientific publications.



**David Jui-Yang Feng** received the B.S. degree in electrical engineering from National Taiwan Ocean University, Keelung, Taiwan, in 2000, and the Ph.D. degree in electro-optical engineering from National Sun Yat-sen University, Kaohsiung, Taiwan, in 2008, where his major research included the MBE-growth of multifunction modulation-doped InGaAlAs/InP strain-balanced multiple quantum wells (MQWs), In(Ga)As/GaAs quantum dots, AlGaAs/GaAs superlattice/MQWs infrared photodetectors, and the compact waveguide coupler for photonic integrated circuits.

He joined the Department of Photonics, National Chiao Tung University, as a Post-Doctoral Researcher, in 2009, and worked in the area of GaN-based photonic devices. In 2013, he went to the University of Maryland at Baltimore County, Baltimore, as a Visiting Scholar, and worked in the MOCVD-growth of quantum cascade lasers and fabricating DFB structures. He has been an Electrical Engineering Department Faculty Member with the National University of Kaohsiung, Kaohsiung, since 2010. He currently works in the area of III-V solar cells, thin-film flexible photonic devices, and supercritical fluids technology.



**Fow-Sen Choa** (M'88–SM'93) received the B.S. degree from National Taiwan University, Taiwan, in 1980, and the M.S. and Ph.D. degrees from the State University of New York, Buffalo, in 1988, all in electrical engineering.

After his Ph.D. research work on femtosecond infrared lasers and detectors, in 1988, he joined AT&T Bell Labs, Holmdel, and Murray Hill, NJ, and worked in the area of photonic integrated circuits and chemical beam epitaxy. Since joining the University of Maryland at Baltimore County (UMBC) in 1991, he has been working in the areas of III-V compound semiconductor material growth and processing, broadband optical switches, RF-photonic components and systems, quantum cascade lasers, photon counting avalanche photodiodes and arrays, photoacoustic sensing, imaging, acoustic array transmissions and receiving, and brain circuit monitoring and stimulations. Since 1991, he has sponsored and co-sponsored with a total of more than U.S. \$14 million in research funding from different sources, including an MOCVD crystal growth facility built at UMBC. He has authored or co-authored over 300 refereed publications.

Prof. Choa is a fellow of the Optical Society and the International Society for Optics and Photonics, and an Associate Editor of the *Journal of High Speed Networks*. He has been a Topical Editor of *Optics Letters* for six years.